Electronic Supplementary Material (ESI) for ChemComm.

Retarded sodium alloying interface reaction for stable anode-less sodium metal batteries

Hao Wu, [#a] Chunlin Xie, [#a] Mingze Zhang, [a] Jiapeng Zou, [a] Runxin Feng, [a] Hongqin Lu, [a] Qi Zhang, [a] Yougen Tang, [a] Haiyan Wang [a]*

[a.] Hunan Provincial Key Laboratory of Chemical Power Sources

College of Chemistry and Chemical Engineering

Central South University

Changsha, 410083, P.R. China

# These authors contributed equally to this work.

E-mail: wanghy419@csu.edu.cn

Methods

Material preparation.

The sodium discs of 12 mm diameter, glass fibre (Whatman GF/A) and Celgard C200 membrane were purchased from Canrd Technology Co. Ltd. Single-sided carbon coated aluminium foil (Al@C foil) purchased from Jinghong New Energy Co. The electrolyte was obtained by dissolving 1 M $NaPF_6$ (DoDoChem, battery grade) in diglyme (DoDoChem, battery grade). The carbon-coated $Na_3V_2(PO_4)_3$ cathode (NVP) was purchased from Shenzhen Kejing Ltd. The composition of the cathode slurry was 90wt% active materials, 5wt% Super P and 5wt% PVDF. The electrode slurries were cast on Al@C foil followed by a drying process under a vacuum. The mass loading of cathode material was about 15~19 mg cm^{-2}.

The metal lead and antimony target with a diameter of 10 cm (99.99% purity) were purchased from ONA Targets Ltd. Magnetron sputtering equipment manufactured by TAILONG ElECTRONICS (Sputter-100). A uniform layer of Pb and Sb was sputtered on the Al@C foil by magnetron sputtering with the sputtering parameters of 200W for 3 min (RF power). The vacuum of the chamber before sputtering was about 1×10^{-5} Pa, the flow rate of Ar gas used for sputtering was 100 sccm, and the rotational speed of the base was 10 r/min.

Characterizations.

Nondestructive-XRD spectra enabling avoidance of air contact were recorded using a Rigaku X-ray diffractometer. The scanning electron microscope (SEM, JSM-7610FPlus) with non-destructive transfer capability was used to characterize the sodium plating and stripping morphology of the substrate. Optical microscopy (AOSVI M203-HD228S) was used to observe the evolution of sodium deposition in glove box. Transmission electron microscopy (TEM, JEOL/JEM-F200) was used to characterize

the crystal structure of the nano-coated layers before and after the alloying reaction. Molybdenum mesh microgrids were coated with Nano-Pb layers using the magnetron sputtering method. The parameters of magnetron sputtering were adjusted to match the process parameters for the preparation of Pb-Al@C, but the sputtering time was shortened to a quarter of the time to meet the requirements for sample thickness in TEM testing. To investigate the structural changes of the coating after sodium plating/stripping, we assembled half-cells for repeated sodium plating/stripping using sputter-coated molybdenum mesh as electrodes. Afterward, a simple solvent cleaning was conducted to coated microgrids before direct utilization for TEM observations. In this work, non-destructive transfer devices were used for SEM, and XRD tests, which adequately preserved the true information of the test samples (the samples were handled in a glove box). The corresponding non-destructive transmission device and the process used are shown below (Figure D1-2):

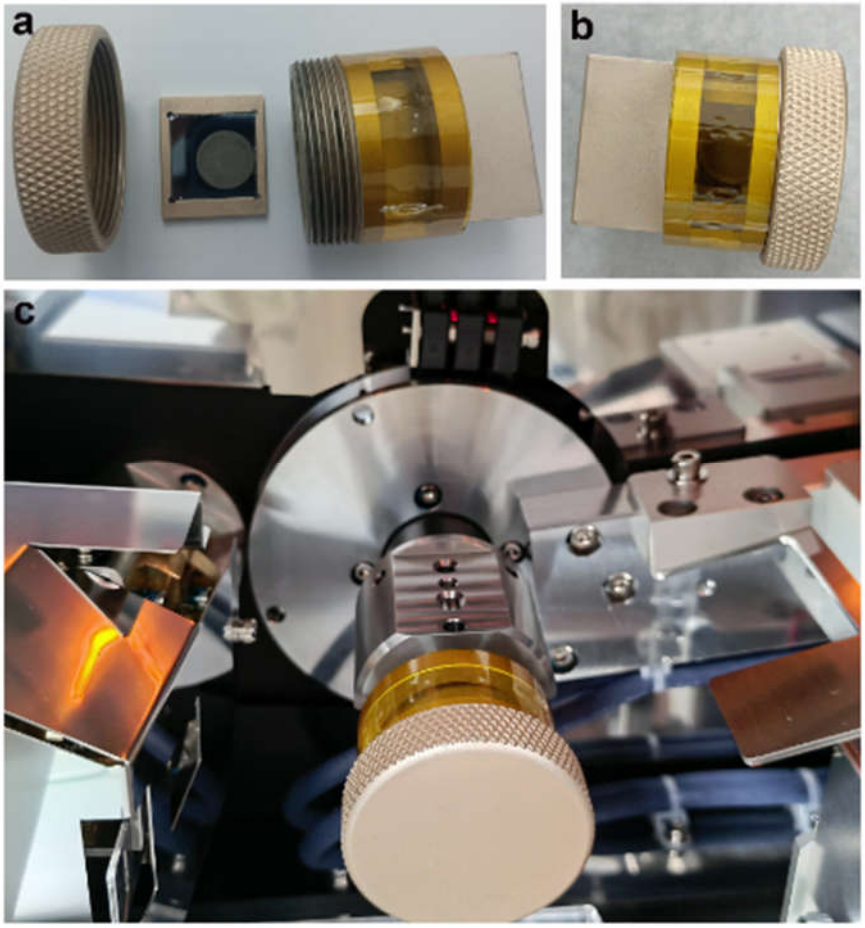

Figure D1. Non-destructive transfer devices for XRD.

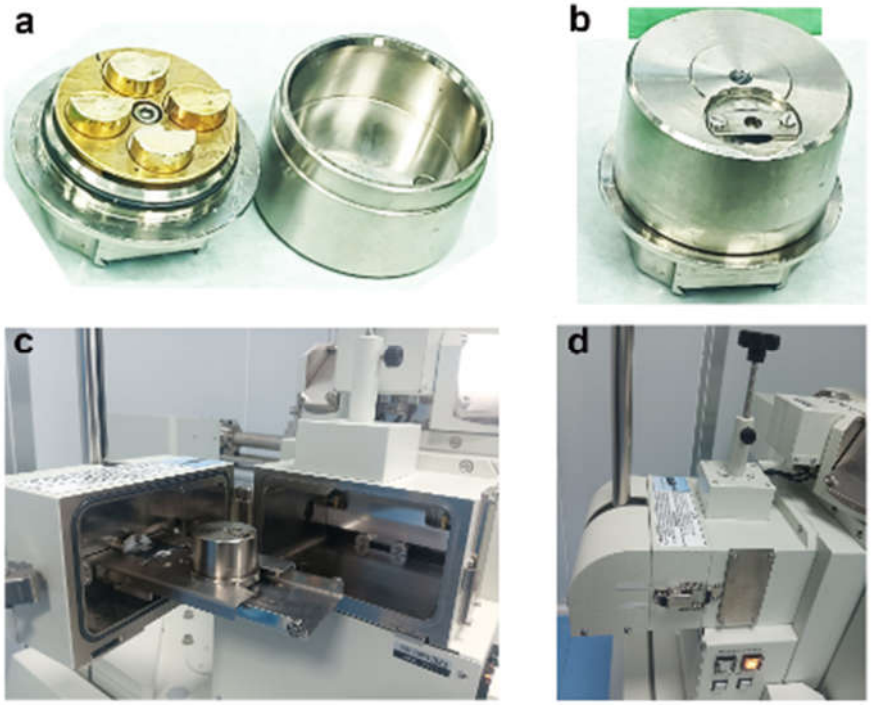

Figure D2. Non-destructive transfer devices for SEM.

Electrochemical measurements.

Coin cells (CR2032) were assembled in an argon-filled glove box. The amount of electrolyte used for a coin cell is about 100 μL. Glass fibre (Whatman GF/A) plus Celgard C200 membrane was utilized as the separator. The galvanostatic charge/discharge tests were performed using a Neware MIHW-200-160CH battery testing system. The anode-less sodium metal battery did not perform any pre-treatment such as pre-sodiumation before cycling. The charge cut-off voltage of the Na||Al@C (or Pb-Al@C and Sb-Al@C) half-cell was set to 0.5 V (vs Na/Na^+). The EIS was performed on the AUTOLAB electrochemical workstation with a frequency range of 0.01 Hz ~500 kHz. The EIS of full cell was tested at full charge state (charged to 3.8V).

Computational details.

The first-principles calculations were conducted using generalized gradient approximation (GGA) and Perdew–Burke–Ernzerhof (PBE) exchange-correlation functional in Castep module of Materials Studio of Accelrys Inc. During geometry optimization, the convergence tolerance was set to 1.0×10^{-5} eV per atom for energy, 3.0×10^{-2} eV $Å^{-1}$ for maximum force, and 1.0×10^{-3} Å for maximum displacement. The binding energy (E_b) of the metal substrate was calculated using a five-layer 3×3 supercell and releasable top three-layer atoms, the carbon structure was modelled using a single layer of graphite (2 × 2 facet) and the corresponding binding energy was calculated according to the following equations:

$$E_b = E_{total} - E_{sub} - E_{atom} \qquad (1)$$

E_{total}, E_{sub}, and E_{atom} represent the total energy of the Pb facets (or Sb, C and Al facets) combined with the sodium atom, the energy of Pb facets (or Sb, C and Al facets), and the energy of the sodium atom, respectively.

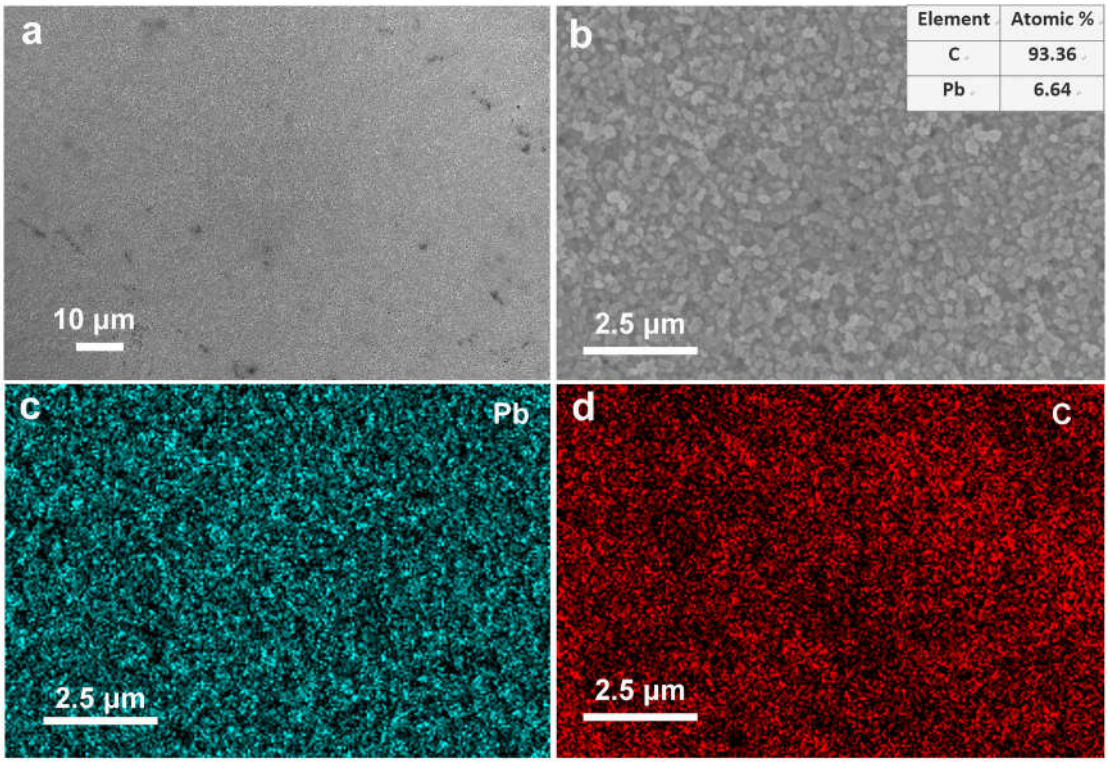

Figure S1. SEM images and corresponding EDS mappings of Pb-Al@C.

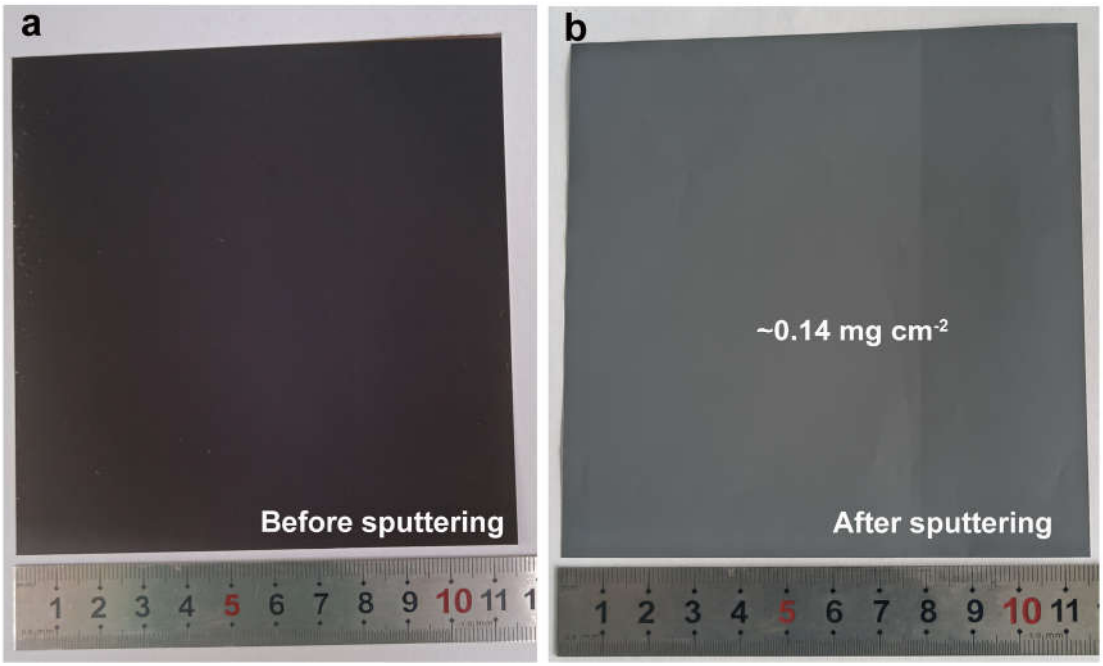

Figure S2. Digital photos of Al@C before and after sputtering of Pb.

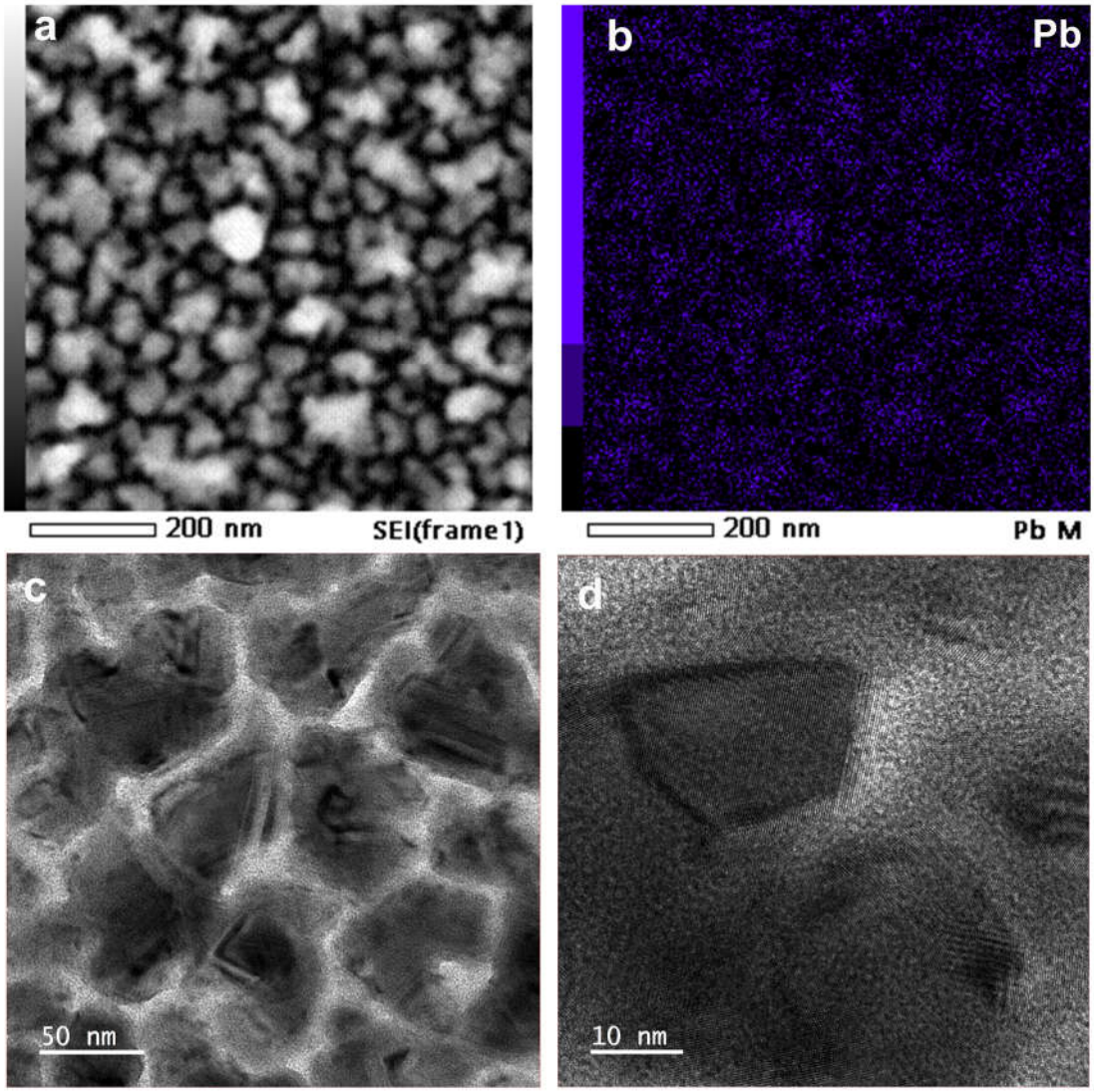

Figure S3. TEM images and corresponding EDS mapping of Pb sputtered on a molybdenum mesh.

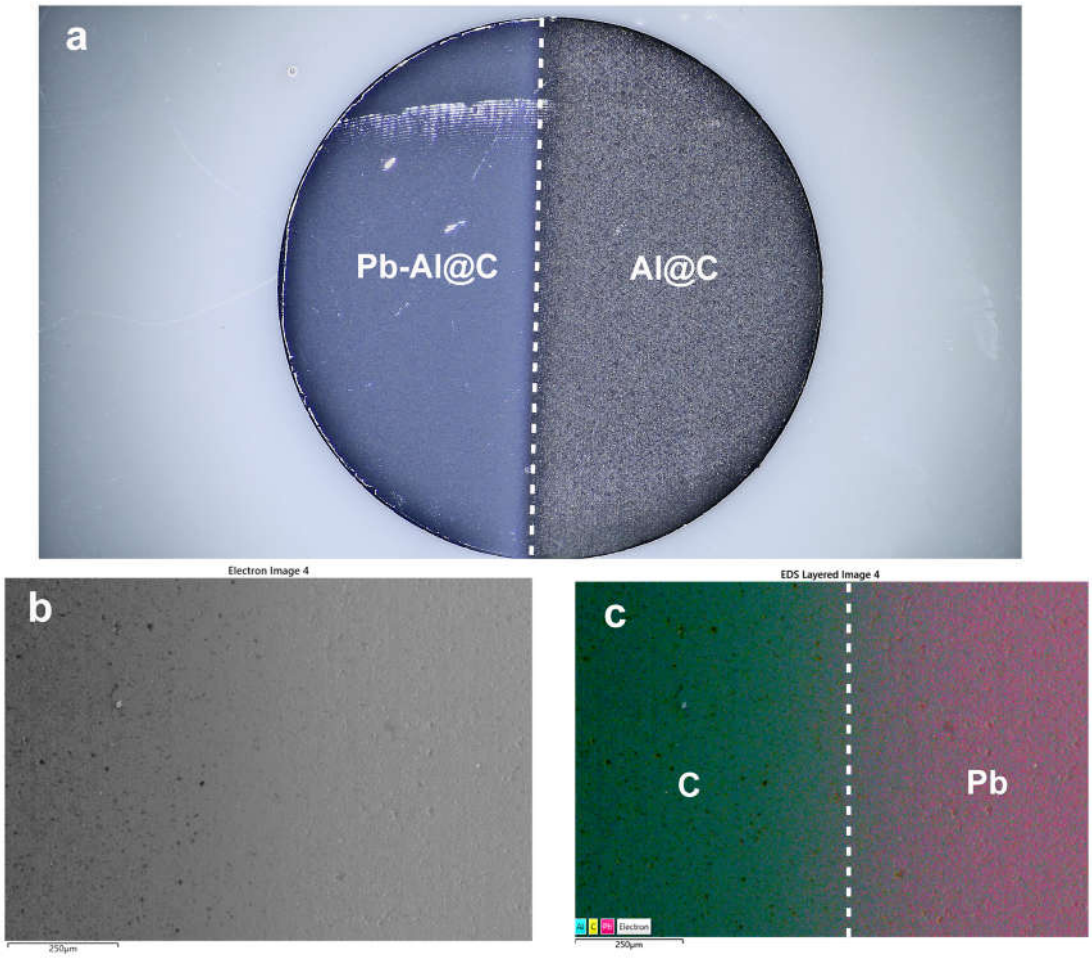

Figure S4. Optical micrographs and EDS mapping of Al@C after selective sputtering.

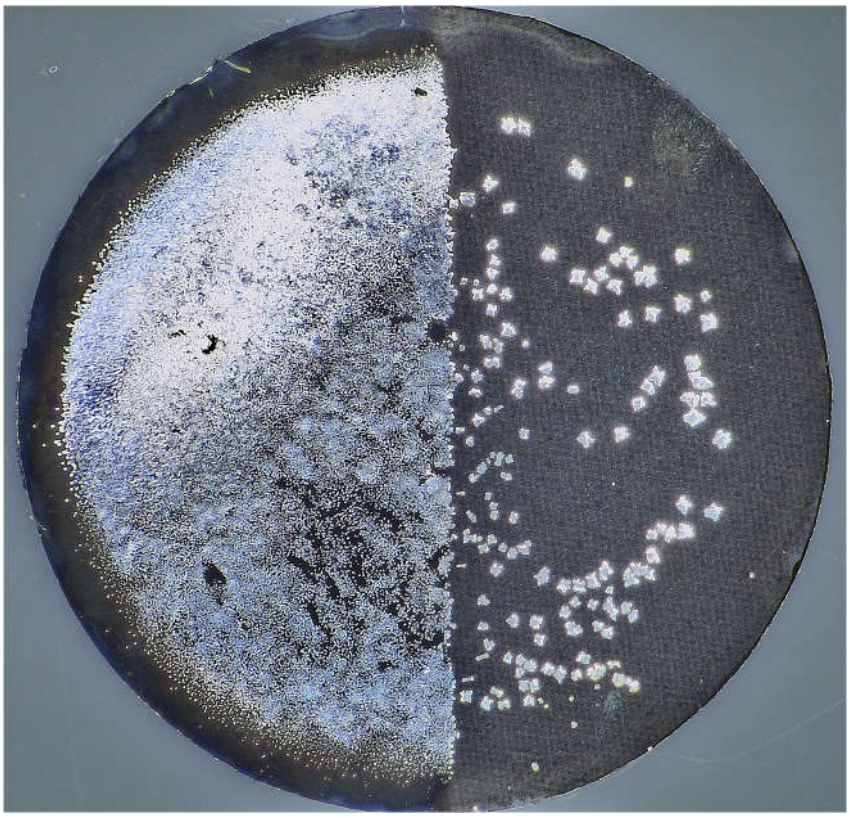

Figure S5. The optical microscope image of the substrate in Figure S4 after deposition of sodium at 1 mA cm^{-2} for 0.4 mAh cm^{-2}.

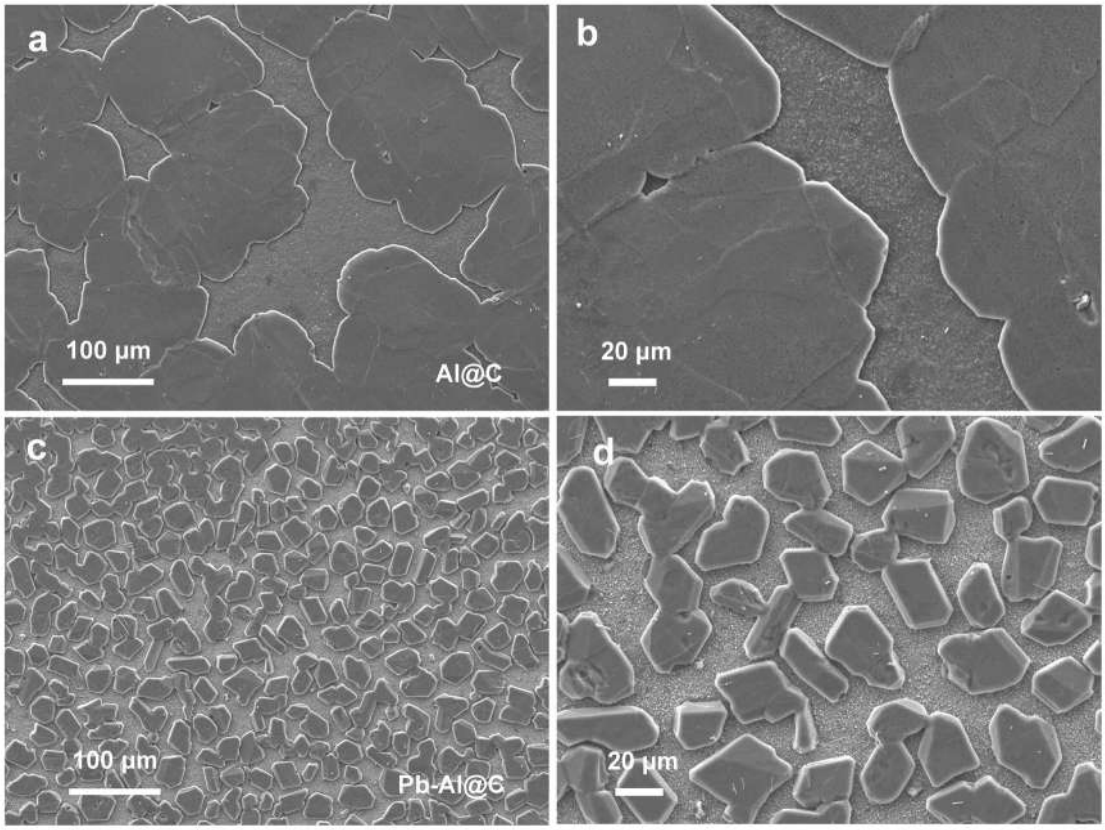

Figure S6. SEM images of sodium deposition on (a-b) Al@C foil and (c-d) Pb-Al@C at 1 mA cm^{-2} for 0.5 mAh cm^{-2}.

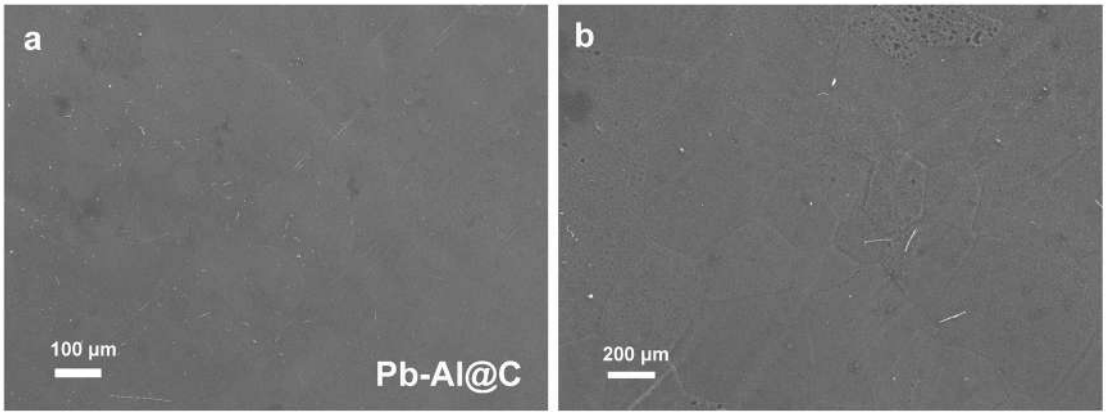

Figure S7. SEM images of sodium deposition on Pb-Al@C at 1 mA cm^{-2} for 2 mAh cm^{-2}.

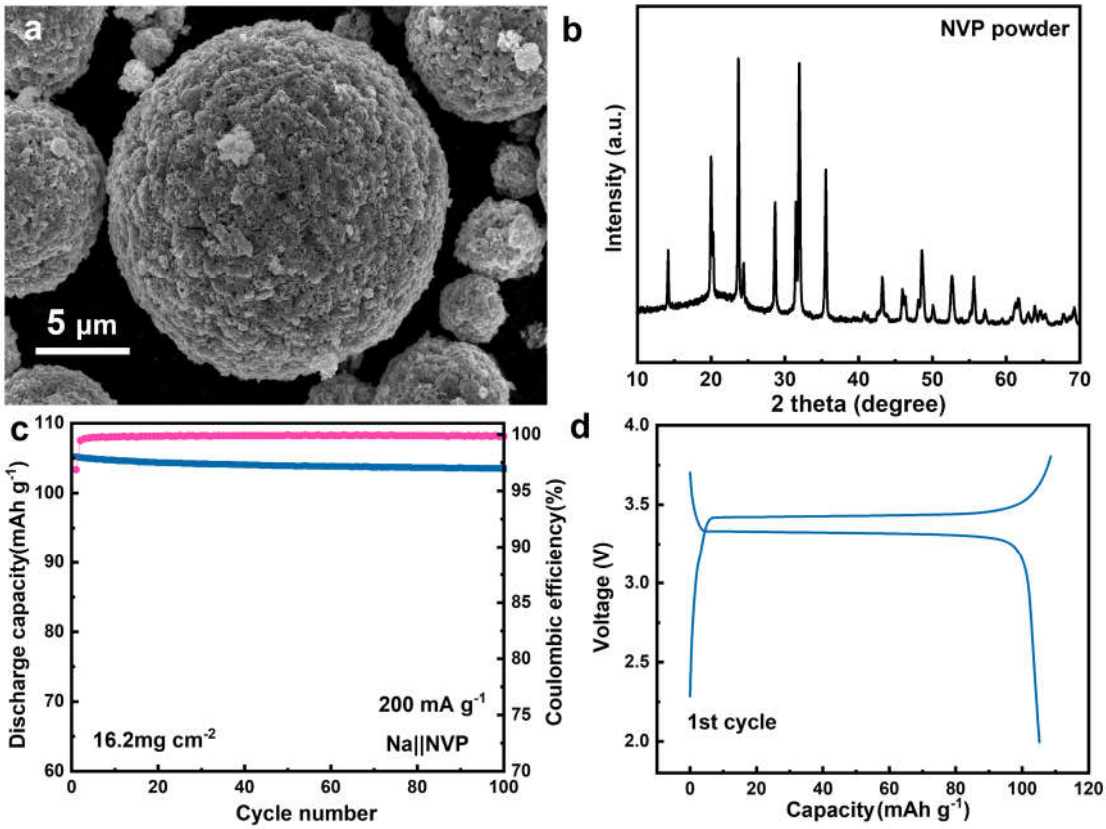

Figure S8. (a) SEM image and (b) XRD pattern of NVP cathode, (c) the cyclic performance and (d) the corresponding initial capacity-voltage curve of the Na||NVP cell.

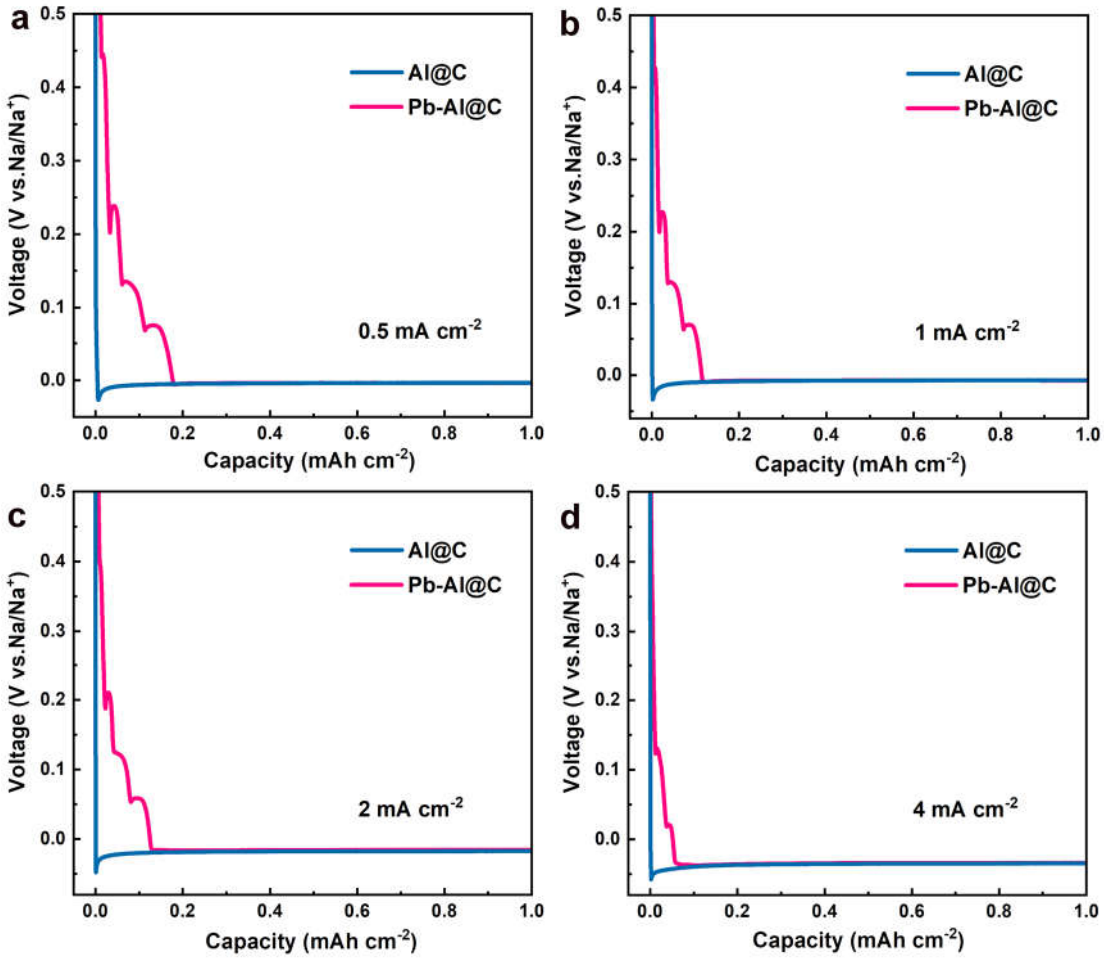

Figure S9. The initial capacity-voltage curves of Na||Al@C and Na||Pb-Al@C half-cells at different current density.

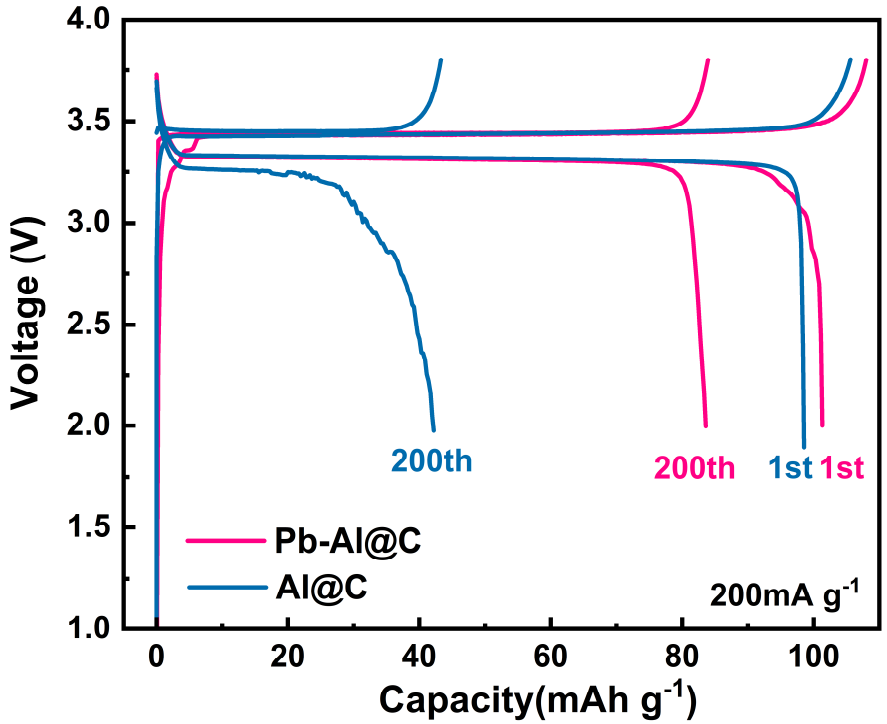

Figure S10. The capacity-voltage curves of Al@C||NVP cell and Pb-Al@C||NVP cell at 200 mA g^{-1} current density.

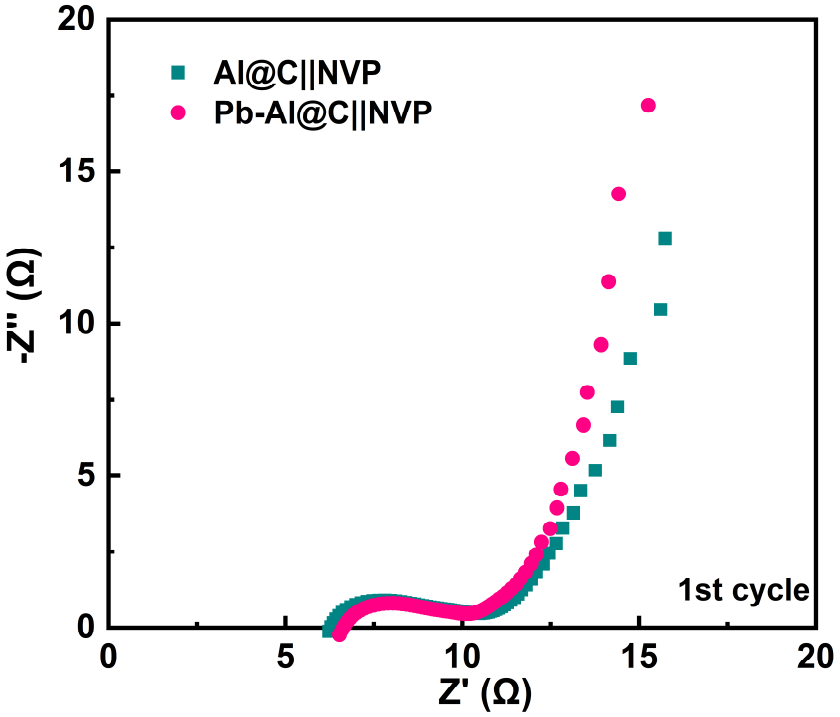

Figure S11. The EIS of Al@C||NVP and Pb-Al@C||NVP cells in the fully charged state for the first cycle.

Figure S12. The anode-side SEM image and the corresponding EDS mappings of Al@C||NVP cell after 100th cycle at 100 mA g^{-1} in a fully discharged state.

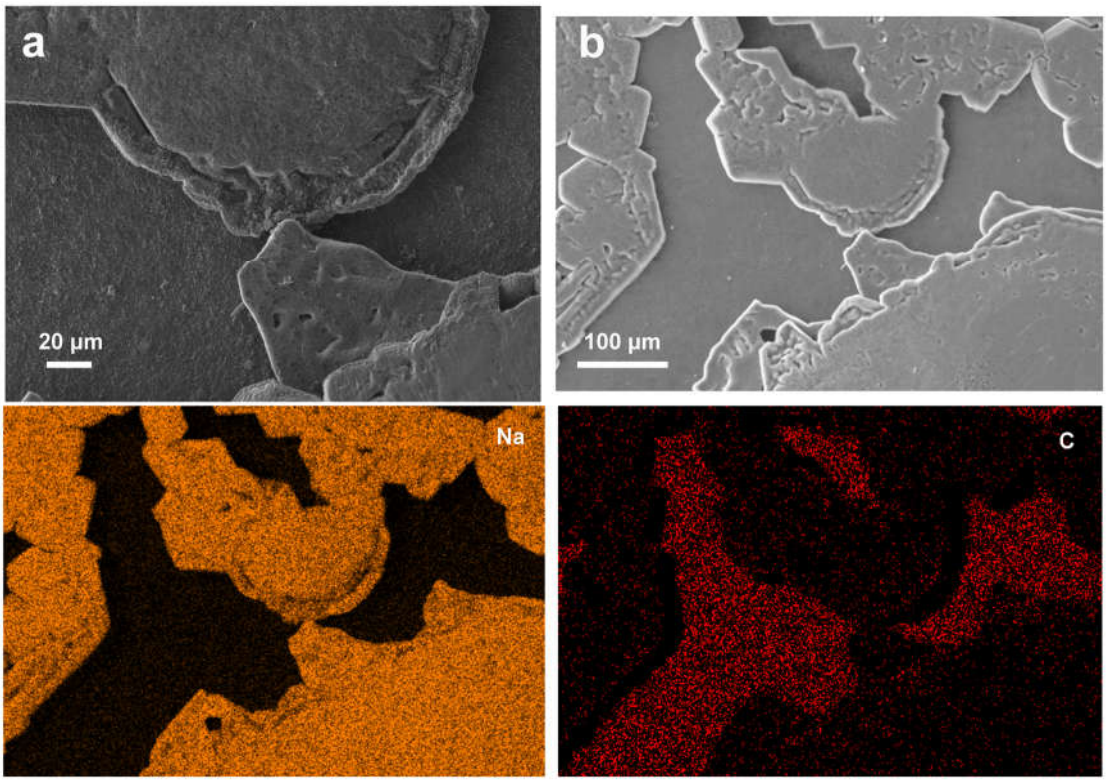

Figure S13. The anode-side SEM images and the corresponding EDS mappings of Al@C||NVP cell after 100th cycle at 100 mA g^{-1} in a fully charged state.

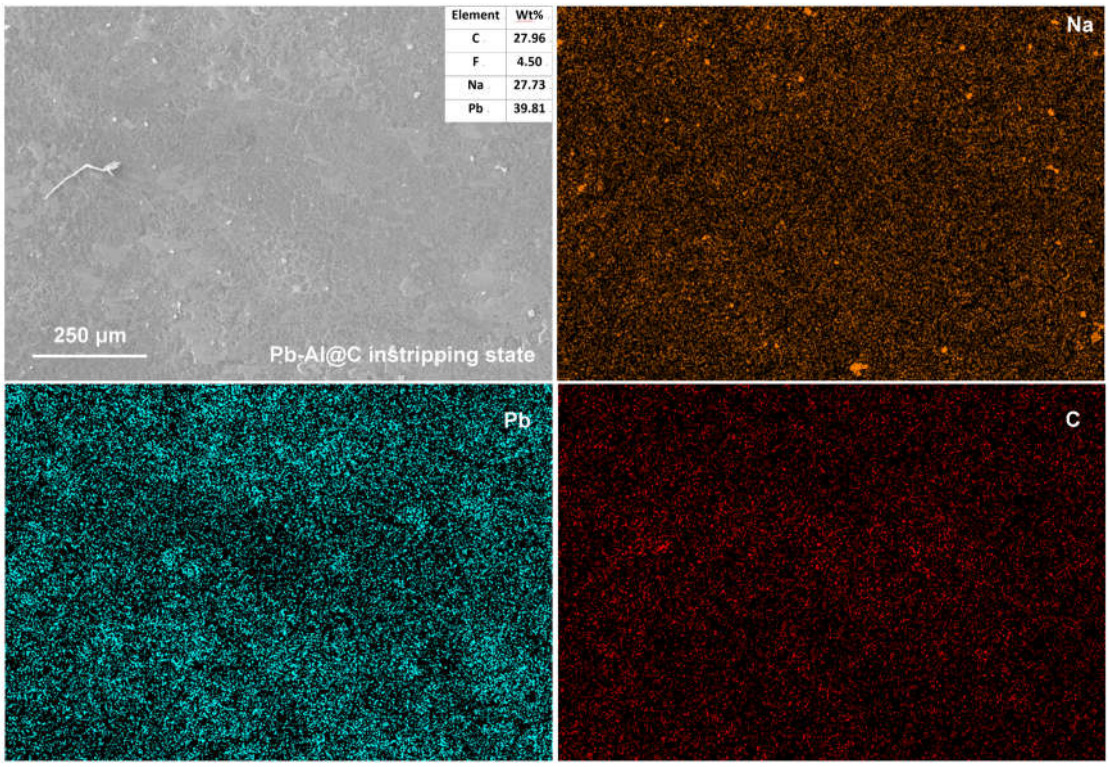

Figure S14. The anode-side SEM image and the corresponding EDS mappings of Pb-Al@C||NVP cell after 100th cycle at 100 mA g^{-1} in a fully discharged state.

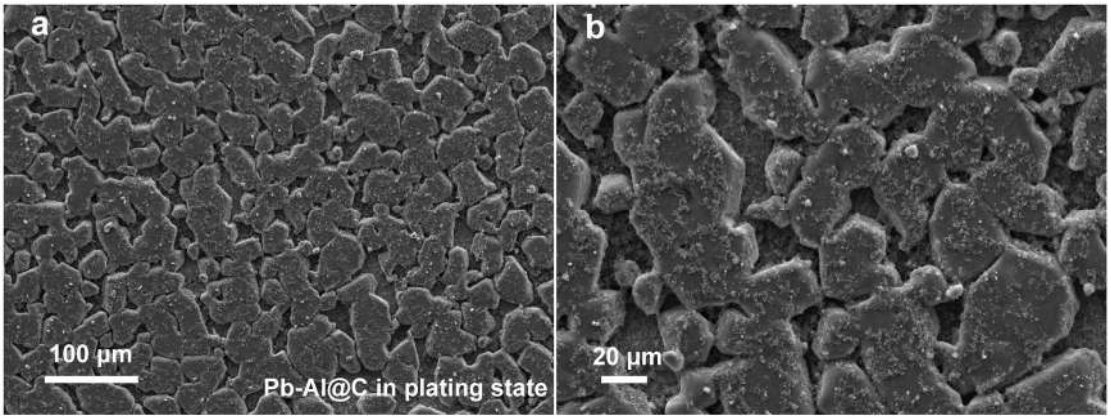

Figure S15. The anode-side SEM images of Pb-Al@C||NVP cell after 100th cycle at 100 mA g^{-1} in a fully charged state.

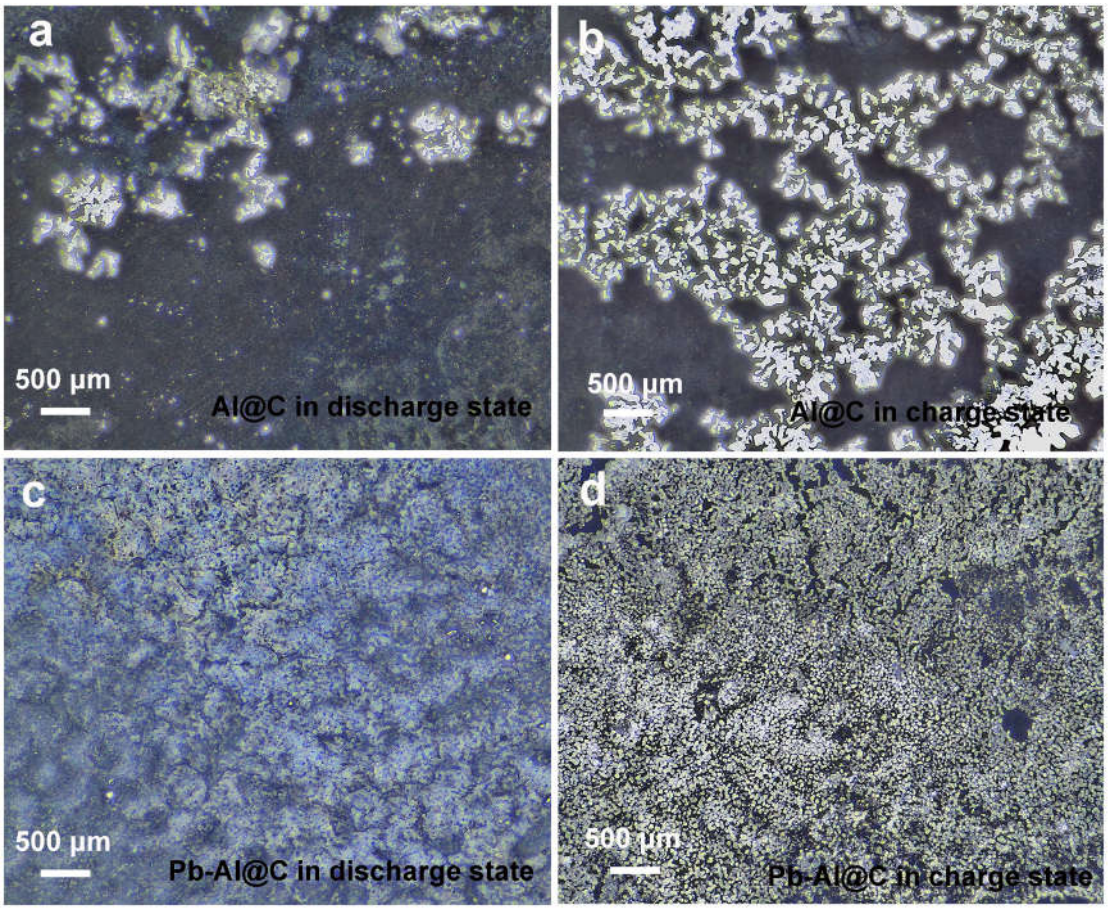

Figure S16. The anode-side optical microscope images of Al@C||NVP cells after 100th cycle at 100 mA g^{-1} in a (a) fully discharged state and (b) fully charged state, the anode-side optical microscope images of Pb-Al@C||NVP cells after 100th cycle at 100 mA g^{-1} in a (c) fully discharged state and (d) fully charged state.

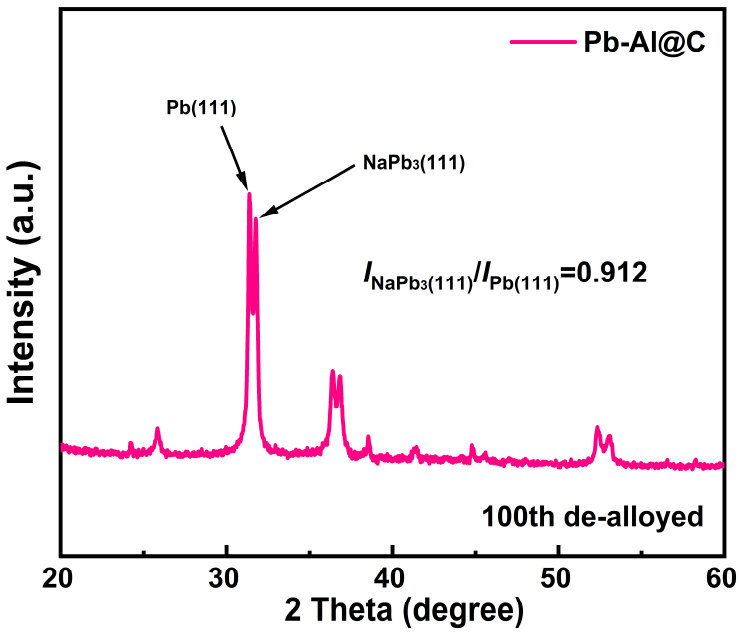

Figure S17. XRD patterns of de-alloyed Pb-Al@C substrates after 100th cycle (half-cell charged to 0.5 V).

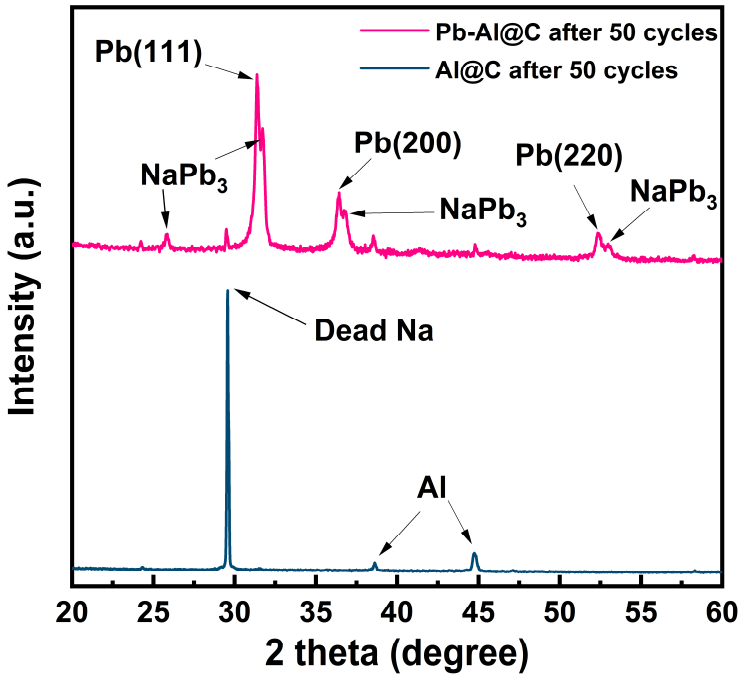

Figure S18. The anode-side XRD patterns of Al@C||NVP and Pb-Al@C||NVP cells after 100th cycle at 100 mA g^{-1} in a fully discharged state.

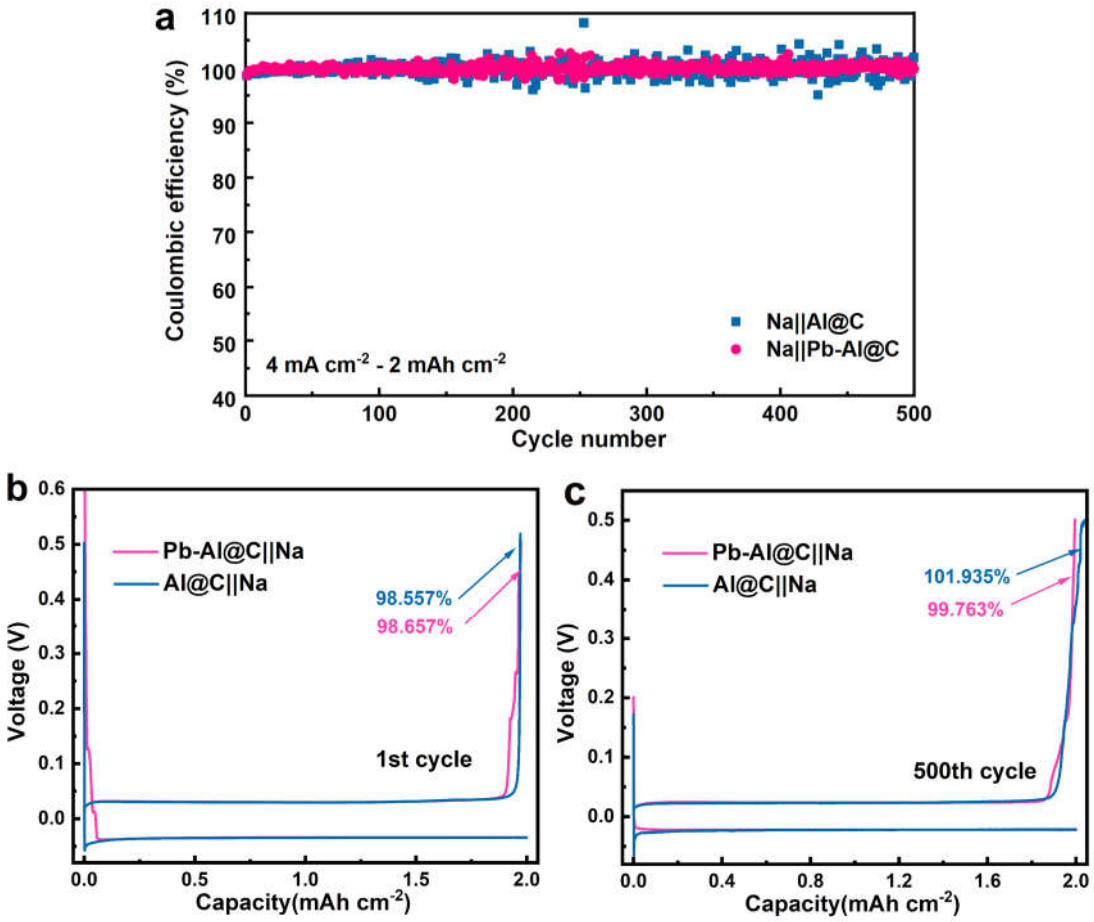

Figure S19. Coulombic efficiency of half-cells at different cycles 4 mA cm^{-2} for 2mAh cm^{-2}.

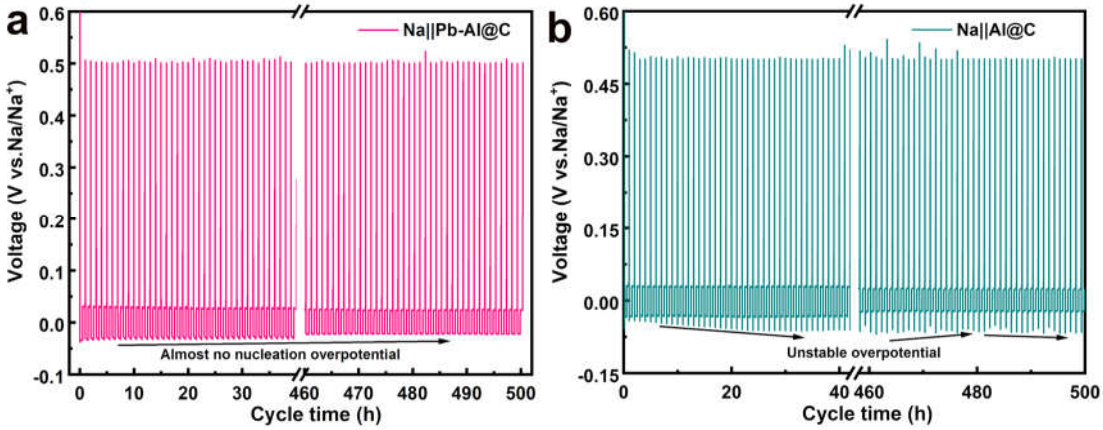

Figure S20. Time-voltage curves of Na||Pb-Al@C and Na||Al@C half-cells at 4 mA cm^{-2} for 2mAh cm^{-2}.

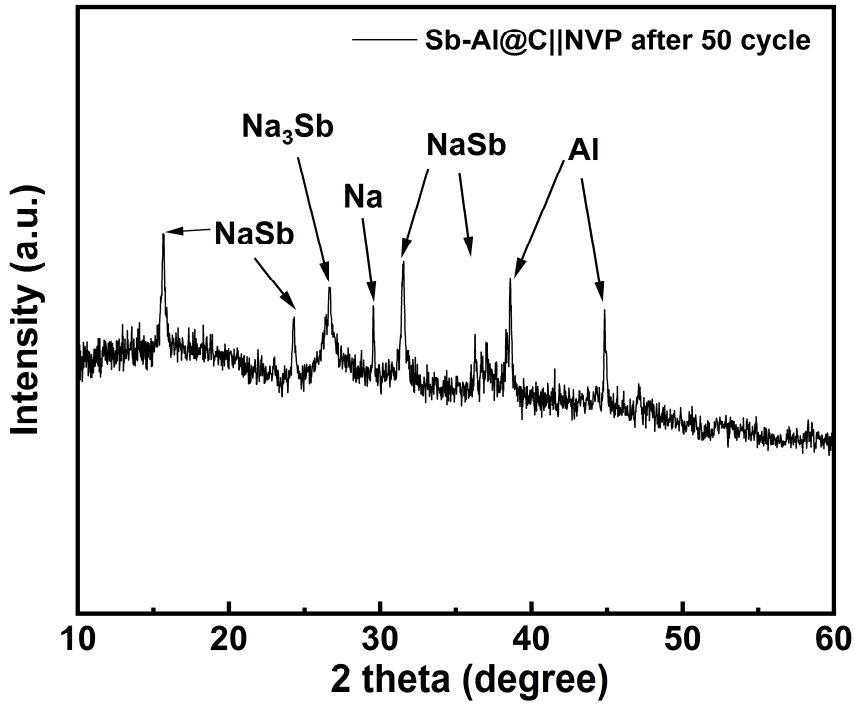

Figure S21. The anode-side XRD pattern of Sb-Al@C||NVP cell after 100th cycle at 100 mA g^{-1} in a fully discharged state.

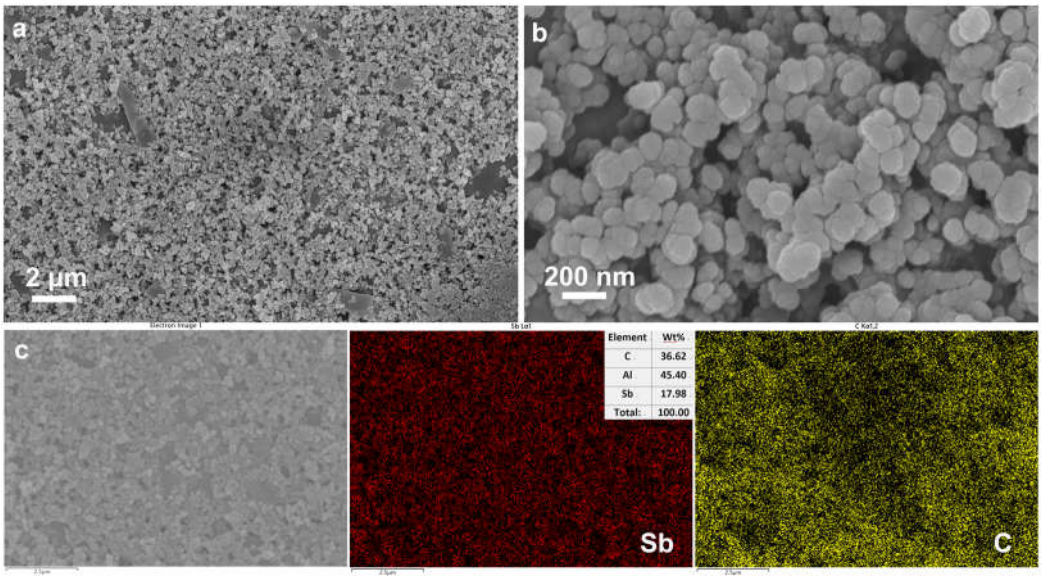

Figure S22. SEM images and corresponding EDS mappings of Sb-Al@C.

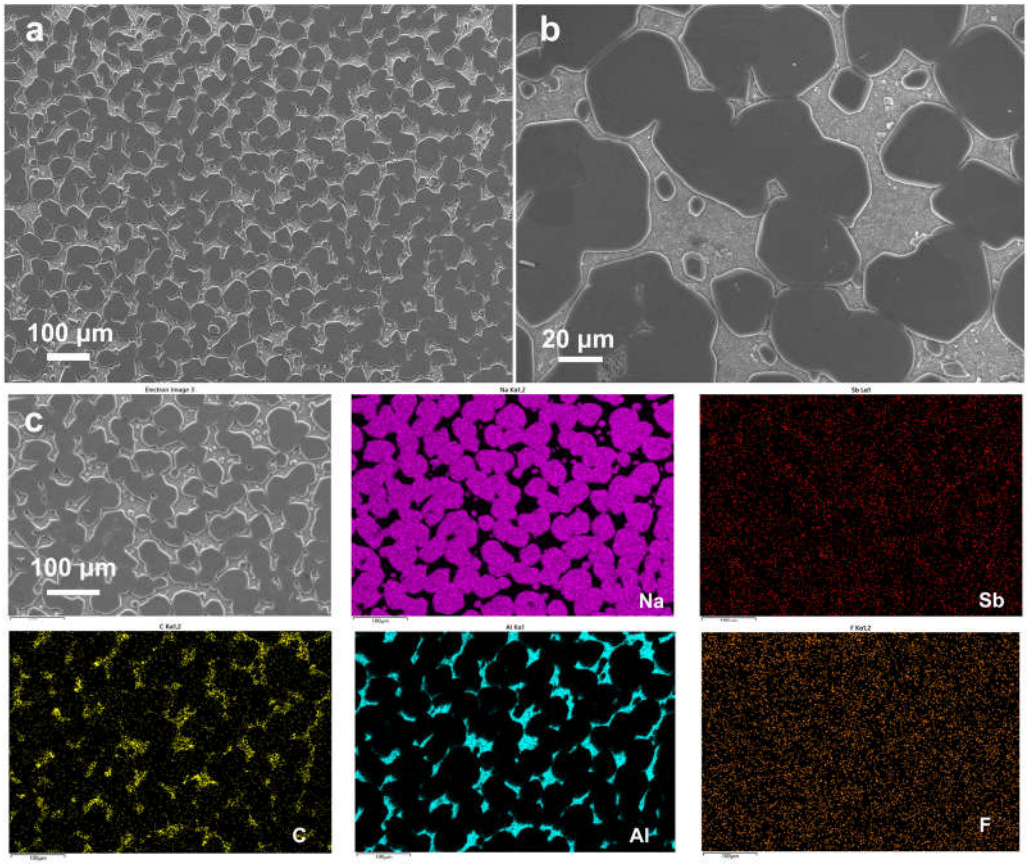

Figure S23. SEM images and corresponding EDS mappings of sodium deposition on Sb-Al@C at 1 mA cm^{-2} for 0.5 mAh cm^{-2}.

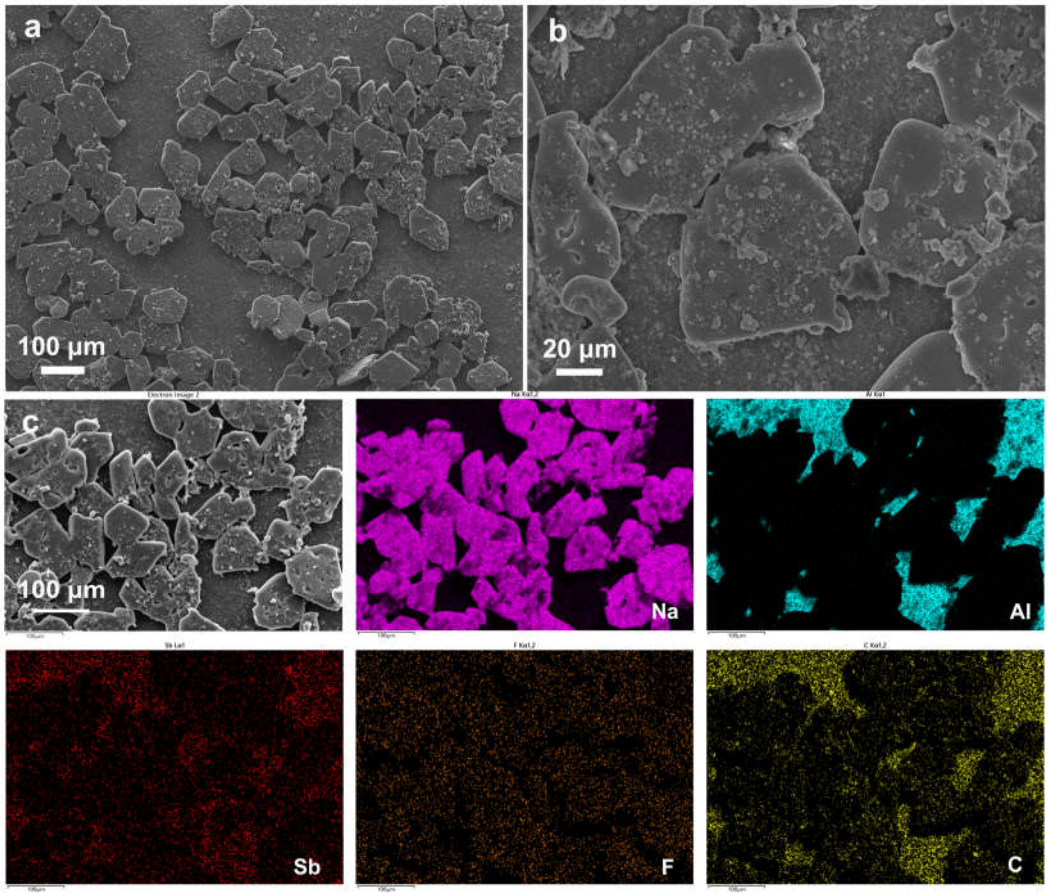

Figure S24. The anode-side SEM images and corresponding EDS mappings of Sb-Al@C||NVP cell after 100th cycle at 100 mA g^{-1} in a fully charged state.

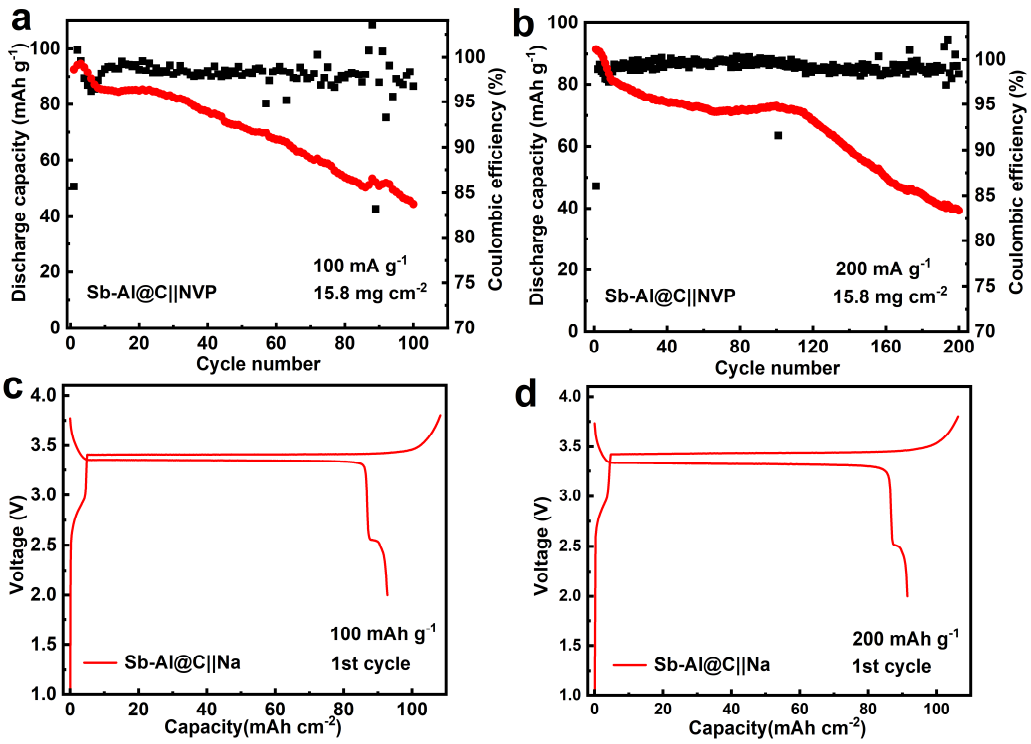

Figure S25. Cyclic performance of Sb-Al@C||NVP cells at (a) 100 mA g^{-1} and (b) 200 mA g^{-1}.

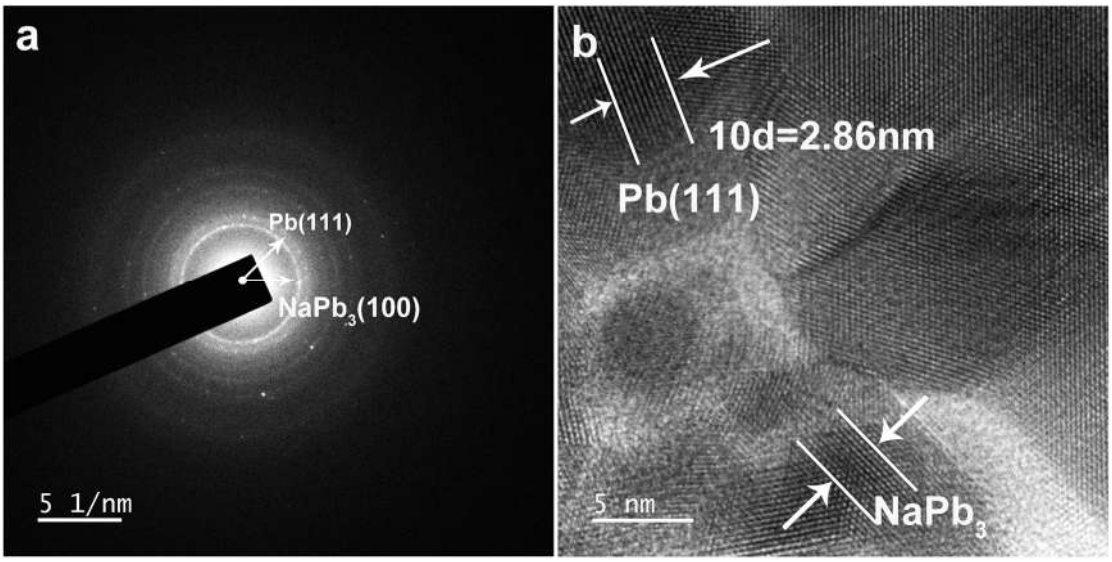

Figure S26. The electron diffraction image and TEM image of Pb particle on molybdenum mesh after 20 cycles of sodium plating/stripping (in the stripped state).

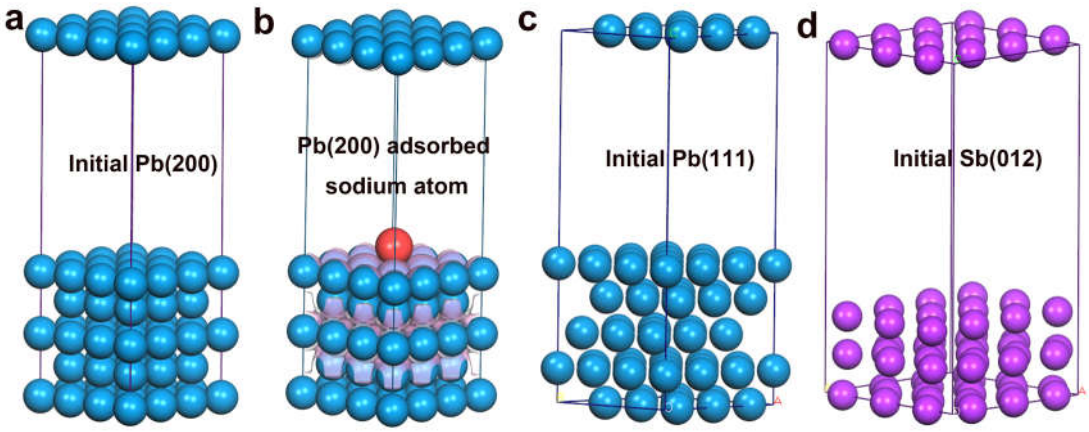

Figure S27. Lattice states of Pb (2 0 0) facets (a) before and (b) after adsorption of sodium atoms. Initial lattice states of the (c) Pb (1 1 1) and (d) Sb (0 1 2) facets.

Table S1. The fitted circuit diagram and the corresponding resistance values of the EIS. Where *F* is the frequency at the top of the charge transfer semicircle.

	R_e **(Ω)**	***Rct*** **(Ω)**	***F*** **(Hz)**	**Equivalent circuit diagrams**
Al@C||NVP-100th cycle	5.11	10.5	794.33	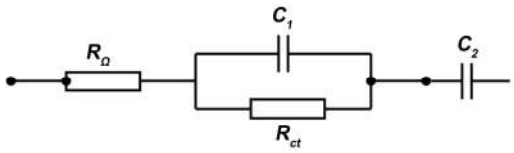
Pb-Al@C||NVP-100th cycle	5.01	4.8	3981.1